Probabilistic evaluation of the one-dimensional Brinson model's sensitivity to uncertainty in input parameters

Ernur Karadoğan, Ph.D.

School of Engineering & Technology, Central Michigan University, Mount Pleasant, MI 48858 USA (e-mail: ernur.karadogan@cmich.edu; Tel: 1 (989) 774 4053)

Abstract

Brinson model is one of the most widely used Shape Memory Alloy models due to its prediction power over a wide range of operating temperatures and inclusion of measurable engineering variables. The model involves parameters that are determined based on experimental data specific to a particular alloy. Therefore, it is subject to both experimental uncertainty and natural random variability in its parameters that propagate throughout the loading/unloading of the material. In this paper, we analyse the sensitivity of the Brinson model to its parameters using a probabilistic approach, and present how the uncertainties in these parameters at different operating temperatures propagate as evidenced by the resulting stress-strain curves. The analyses were performed for isothermal loading/unloading and at various operating temperatures representing possible phase changes between martensite-austenite and martensite-martensite variants. The results show that the sensitivity of the model varies considerably based on the operating temperature and loading conditions. Additionally, the variability in the model's output is amplified after phase transitions during loading, and loading the material above the critical stress for martensite transition reduces variability during unloading. Based on the results of the sensitivity analysis, recommendations as to which parameters affect the variability of the model-predicted stress-strain curves are presented.

Introduction

Shape Memory Alloys (SMAs) have drawn significant attention due to their characteristics that have potential to revolutionize the engineering design and related applications (Jani et al., 2014). They have been used as functional materials and in the development of novel actuators that can be used in active control of structures. SMAs have been used in a wide variety of applications due to their high recovery stress (>500 MPa) (Song et al., 2003; Balta et al., 2005), low operation power, large recoverable strain (up to 10 %) (Wei et al., 1998), and long life span under cyclic loading (Ikuta, 1990). Additionally, SMAs have very high power volume ratio that attests to their tremendous potential to be used in compact design solutions (Balta et al., 2005).

The application areas of SMAs can be broadly divided into two groups as medical and nonmedical applications. After the discovery of the shape memory effect in 1962 (Buehler et al., 1963), one of the first applications of SMAs was in dentistry; first superelastic braces were made from nitinol (NiTi) (Andreasen, 1977; Andreasen and

Hilleman, 1971). It was not until after a surgical product, Mitek Anchor, was approved by the FDA in 1989 that SMA has become very popular in biomedical applications. The increase in its popularity has since been driven by their favorable properties such as corrosion resistance (Buehler and Wang, 1968), biocompatibility (Mantovani, 2000; Ryhänen et al., 1998), and physical properties that replicate those of human tissues and bones (Morgan, 2004). Many other applications in medicine included spinal implants (Vena et al., 2005; Wever et al., 2002; Sanders et al., 1993, 1994; Schmerling et al., 1976), bone modeling (Kujala et al., 2002), artificial muscles (Machado and Savi, 2003), aneurysm repair (Uflacker and Robison, 2001; Kaufman et al., 2000), treatment of urinary continence (Tanaka et al., 1999), reconstructive and aesthetic surgery (Khouri and Brava, 2002), and surgical tools (Musialek 1998; Konh, 2015;). Today, nonmedical applications of SMAs can be found in many disciplines including aerospace (Peng et al., 2005; Roh et al., 2005; Prahlad and Chopra, 2001; Birman, 1997; Hartl and Lagoudas, 2007), automotive (Williams et al., 2010; Zychowicz, 1992; Leary et al., 2013; Suzuki, 1986; Brugger et al., 2006), and robotics (Fujita, 1989; Kuribayashi, 1989; Honma and Miwa, 1985; Simone et al., 2015). For instance, some examples of novel biologically inspired robotic systems using SMA actuators are Octopus arm (Cianchetti et al., 2014), Meshworm (Seok et al., 2013), and GoQBot (Lin et al., 2011) with some application (due to their silent and low-power operation) in marine science (Cho et al., 2008; Willy and Low, 2005; Morgansen et al., 2001; Triantafyllou and Triantafyllou, 1995).

SMAs can recover from large strains due to crystallographic transformations between martensite and austenite phases as a function of stress and temperature. In the stress-free state SMAs have four transition temperatures: Martensite finish temperature (M_f), Martensite start temperature (M_s), Austenite start temperature (A_s), and Austenite finish temperature (A_f). It is assumed that there is no phase transformation within the temperature range $M_s < T < A_s$. Depending on the operating temperature of the material, phase transformations occur with changing temperature and loading.

The mechanical behavior of SMAs can be classified into two categories: the shape memory effect and pseudoelastic effect. The shape memory effect refers to the material to remember its original shape after loading and unloading, and to return to the original shape upon heating. As can be seen from Figures 1a and 1b, at temperatures $T < A_f$, a residual strain remains upon unloading, and this residual strain can be recovered by heating the material above its austenite finish temperature. The pseudoelastic effect refers to the recovery of the strain experienced by the material during unloading resulting in a hysteresis loop. As can be seen in Figures 1c and 1d, for temperatures $T > A_f$ the pseuodoelastic effect returns the material to its original shape as no residual strain remains upon unloading. A detailed description of the SMA mechanical behavior can be reviewed in Brinson (1993).

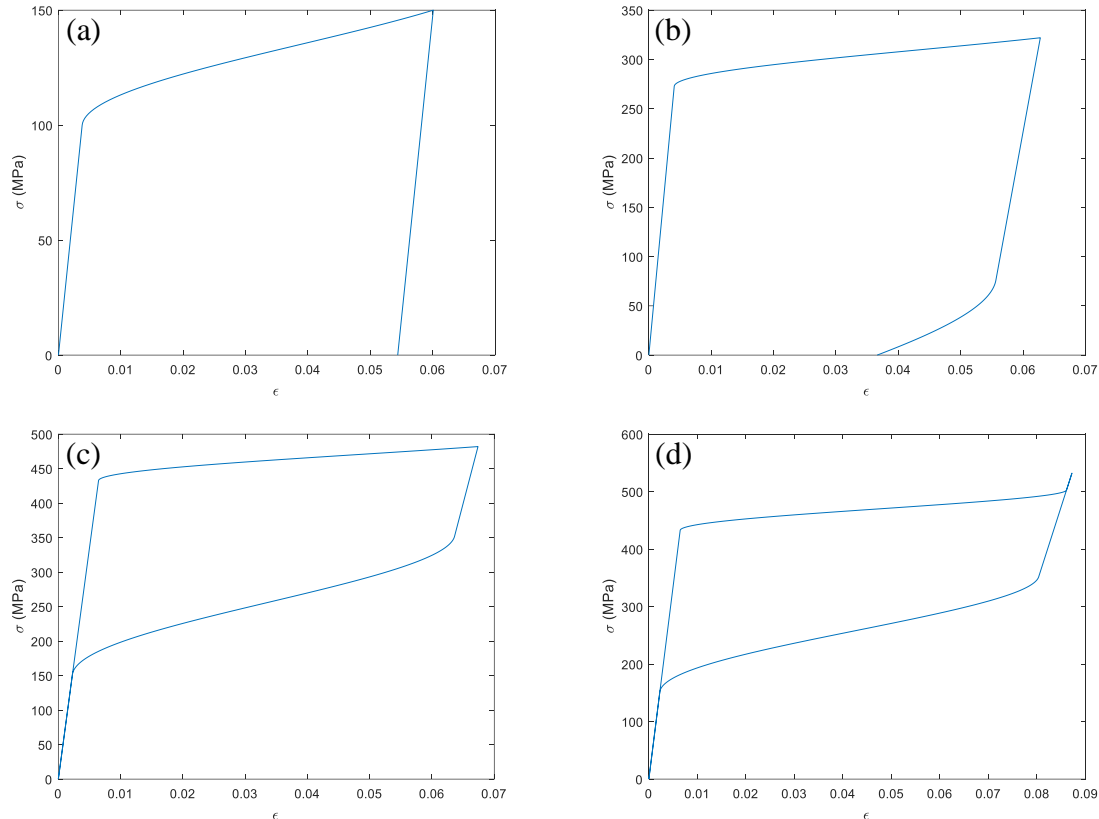**Figure 1** Representations of the shape memory effect: (a) $T < A_s$, (b) $A_s < T < A_f$, and the pseudoelastic effect: (c) $T > A_f$, (d) $T > A_f$ and maximum loading exceeds the critical stress at which the material converts to 100% detwinned martensite when starting from 100% austenite.

As in any material, reliable prediction of stress-strain data from a constitutive model is essential for the applications with SMAs. They affect the calculation of the forces and displacements inside the structure, and, therefore, the overall behaviour of the entire structural model depends on their accurate estimations. For instance, the applications that employ SMAs as actuators require the modelling effort in order to test a controller strategy and tune the controller parameters by means of simulations before implementing any hardware-in-the-loop testing. Proper representation of the plant to be controlled in a simulation environment becomes especially critical when time and cost are limiting factors. Therefore, the aims of this study were: 1) to quantify the effects of parameter uncertainty in the Brinson model on the prediction of stress-strain data over the range of simulated loading/unloading conditions; and 2) to investigate which model parameters are dominant in determining the output variability. A probabilistic approach is employed by representing the input parameters as probability distributions in order to estimate the distributions for the stress-strain data for a selected SMA. The results of the analysis systematically quantifies the sensitivity of the Brinson model to its parameters.

Brinson Model

The Brinson model (Brinson, 1993), developed based on the previous work by Liang (1990) and Tanaka (1986), assumes an internal state variable for the martensite material fraction (ξ) that represents the percentage of the martensite formation. This fraction is a combination of purely temperature-induced martensite and martensite that has been transformed under stress. The total martensite fraction is expressed by:

$$\xi = \xi_S + \xi_T \tag{1}$$

where ξ_S is the fraction of the material that has been transformed into single martensitic variant, and ξ_T is the temperature-induced martensite fraction. This separation of the martensite fraction allows the Brinson model to simulate the thermomechanical behavior of SMAs at temperatures below their martensite start temperature. The stress-strain relationship in the model is expressed by:

$$\sigma - \sigma_o = D(\xi)\epsilon - D(\xi_o)\epsilon_o + \Omega(\xi)\xi_s - \Omega(\xi_o)\xi_{so} + \Theta(T - T_o) \tag{2}$$

where the function $D(\xi)$ is representative of the modulus of the SMA material, $\Omega(\xi)$ is considered the transformation tensor, and Θ is related to the thermal coefficient of expansion for the SMA material, which is assumed to be constant, σ and ϵ are the stress and strain developed in the material, respectively. The initial conditions for stress, strain, martensite material fraction, and stress-induced martensite fraction are represented by σ_o, ϵ_o, ξ_o, and ξ_{so}, respectively. The modulus and the transformation sensor are functions of the martensite fraction:

$$D(\xi) = D_a + \xi(D_m - D_a) \tag{3}$$

$$\Omega(\xi) = -\epsilon_L D(\xi) \tag{4}$$

where D_m is the modulus value for the SMA as 100% martensite, D_a is the modulus value for the SMA as 100% austenite, and ϵ_L is the maximum residual strain that can be recovered, which is assumed to be a material constant (Perkins et al., 1975). The phase transformation equations for the Brinson model are provided below (Brinson, 1993):

CONVERSION TO DETWINNED MARTENSITE

for $T > M_s$ and $\sigma_s^{cr} + C_M(T - M_s) < \sigma < \sigma_f^{cr} + C_M(T - M_s)$:

$$\xi_s = \frac{1 - \xi_{so}}{2} \cos\left\{ \frac{\pi}{\sigma_s^{cr} - \sigma_f^{cr}} \times \left[\sigma - \sigma_f^{cr} - C_M(T - M_s) \right] \right\} + \frac{1 + \xi_{so}}{2} \tag{5a}$$

$$\xi_T = \xi_{TO} - \frac{\xi_{TO}}{1 - \xi_{so}}(\xi_s - \xi_{so}) \tag{5b}$$

for T< M_s and $\sigma_s^{cr} < \sigma < \sigma_f^{cr}$:

$$\xi_s = \frac{1 - \xi_{so}}{2}\cos[\frac{\pi}{\sigma_s^{cr} - \sigma_f^{cr}}(\sigma - \sigma_f^{cr})] + \frac{1 + \xi_{so}}{2} \qquad (5c)$$

$$\xi_T = \xi_{TO} - \frac{\xi_{TO}}{1 - \xi_{so}}(\xi_s - \xi_{so}) + \quad \Delta_{T\xi} \qquad (5d)$$

Where, if M_f<T<M_s and T<T_O,

$$\Delta_{T\xi} = \frac{1-\xi_{TO}}{2}\{\cos[a_M(T - M_f)] + 1\} \qquad (5e)$$

Else, $\Delta_{T\xi} = 0$

CONVERSION TO AUSTENITE

for $T > A_s$ and $C_A(T - A_f) < \sigma < C_A(T - A_s)$:

$$\xi = \frac{\xi_o}{2}\left\{\cos\left[a_A\left(T - A_s - \frac{\sigma}{C_A}\right)\right] + 1\right\} \qquad (6a)$$

$$\xi_s = \xi_{so} - \frac{\xi_{so}}{\xi_o}(\xi_o - \xi) \qquad (6b)$$

$$\xi_T = \xi_{TO} - \frac{\xi_{TO}}{\xi_o}(\xi_o - \xi) \qquad (6c)$$

where ξ_{TO} is the initial temperature-induced martensite fraction, C_M and C_A are the slopes of the transition inducing critical stress-temperature curve for austenite to martensite and martensite to austenite transformations, respectively. σ_s^{cr} and σ_f^{cr} are the critical transformation stresses for the martensite variants. Finally, the constants a_M and a_A are expressed by:

$$a_M = \frac{\pi}{M_s - M_f}, \quad a_A = \frac{\pi}{A_f - A_s}. \qquad (7)$$

Methods

The strain values for Ni$_{55}$Ti shape memory alloy were calculated based on simulated stress values using the one-dimensional Brinson model (Figure 2) (Brinson, 1993). The material properties for the alloy are listed in Table 1 (Dye, 1990; Liang, 1990). Five operating temperatures were specified based on the phase transformation temperatures of the material (Table 2). Except for the cases when $T < M_f$ and $M_f < T < M_s$, all simulations were performed with initially 100% austenite, which corresponds to an initial martensite fraction of zero. At temperature $T < M_f$, the material started as 100% martensite with a martensite fraction of one, and at $M_f < T < M_s$, the initial martensite fraction was calculated using Eqn. (5e) as 0.7690. Therefore, only initial nonzero martensite fraction was temperature-induced as a result of cooling from the parent austenite phase. Initial stress-induced martensite fraction were zero in all cases considered.
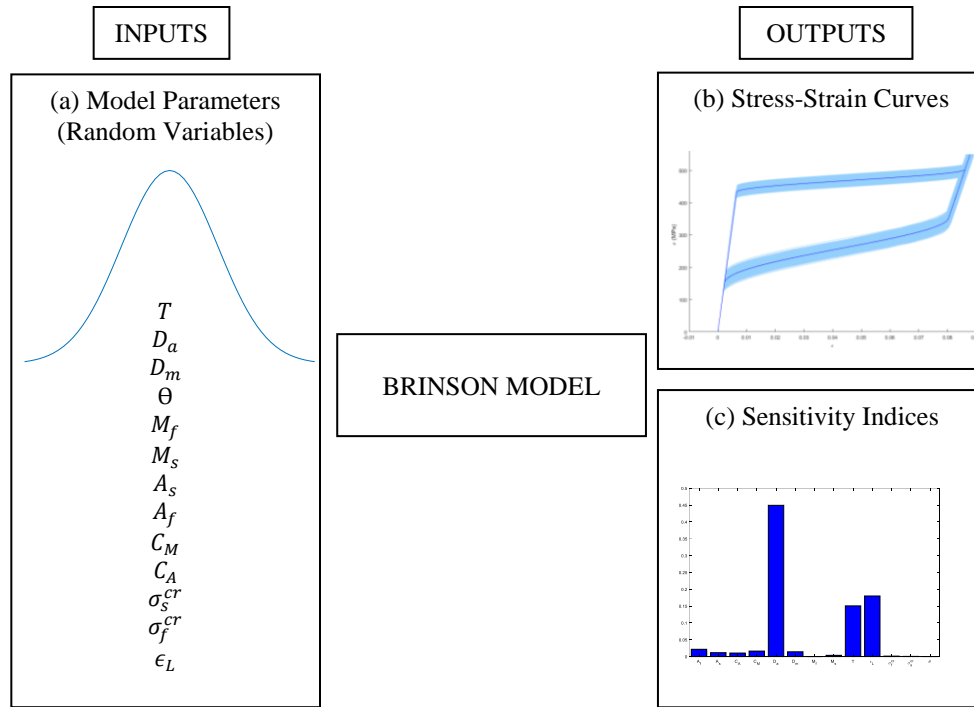
5

INPUTS		OUTPUTS

Figure 2 Uncertainties in the stress-strain curves as determined by the Brinson model were simulated using probabilistic analysis. The probabilistic inputs were (a) the parameters of the model with normal distribution. The outputs included (b) the distribution of the strain at simulated stress values at a given operating temperature, and (c) sensitivity indices of the stress-strain curves to the inputs.

Table 1 $Ni_{55}Ti$ Properties (Dye, 1990; Liang 1990)

Parameter	Description	Deterministic Value	Unit
T	Operating temperature	5, 12, 20, 40, 60	°C
ϴ	Represents the thermal coefficient of expansion	0.55	MPa/°C
D_a	Modulus value as 100% austenite	67,000	MPa
D_m	Modulus value as 100% martensite	26,300	MPa
M_f	Martensite finish temperature	9.0	°C
M_s	Martensite start temperature	18.4	°C
A_s	Austenite start temperature	34.5	°C
A_f	Austenite finish temperature	49.0	°C
C_M	Slope of the transition inducing critical stress-temperature curve for austenite to martensite transformation	8.0	MPa/°C
C_A	Slope of the transition inducing critical stress-temperature curve for martensite to austenite transformation	13.8	MPa/°C
σ_s^{cr}	Critical transformation stress at the start of martensite variants	100.0	MPa
σ_f^{cr}	Critical transfomation stress at the finish of martensite variants	170.0	MPa
ϵ_L	Maximum residual strain that can be recovered upon heating	0.067	-

Table 2 Simulated Operating Temperatures

T (°C)	Description
5	$T < M_f$
12	$M_f < T < M_s$
20	$M_s < T < A_s$
40	$A_s < T < A_f$
60	$T > A_f$

The uncertainty and sensitivity analysis included six cases. Five of these cases corresponded to the aforementioned operating temperatures with a maximum loading stress that was 50 MPa more than the critical transformation stress at the start of martensite variants —the effect of temperature on this critical stress was incorporated in the implementation of the model. The sixth case was added in order to observe the behaviour of the model when the material converts to 100% detwinned martensite when it initially started from 100% austenite. This last case was simulated at 60°C with a maximum loading stress of 550 MPa, which is more than the critical transformation stress at the start of martensite variants at 60°C.

The sensitivity analysis was performed using the Fourier Amplitude Sensitivity Test (FAST) (Cukier et al., 1973, 1975, 1978; Pianosi et al., 2015). FAST is a variance-based sensitivity test that does not have any assumptions in terms of the model structure, and it is reliable for both monotonic and non-monotonic models. Its robustness for nonlinear models also makes it appropriate for the purposes of this study. It effectively considers the entire input space using a search curve that scans the multidimensional space of the input factors. FAST procedure estimates the resulting variance of the model output and the individual contributions of each input parameter, which enables estimation of the sensitivity index of each input independent from the remaining parameters. The procedure does not handle parameter correlations.

Thirteen input parameters were included in this study: operating temperature (T), thermal coefficient of expansion for the SMA material (Θ), the material moduli (D_a and D_m), critical transformation stresses (σ_f^{cr} and σ_s^{cr}), martensite finish temperature (M_f), martensite start temperature (M_s), austenite start temperature (A_s), austenite finish temperature (A_f), the slopes of the transition inducing critical stress-temperature curves (C_M, C_A), and maximum residual strain (ϵ_L). All parameters in the analysis were assumed to have a normal distribution with a coefficient of variation (COV) of 0.01. Higher COV values cause overlapping of the normal distributions assumed for some of the parameters tested (M_f, M_s, A_s, A_f, σ_f^{cr} and σ_s^{cr}), which results in situations that violate the nature of the material and causes constitutive equations to fail. The probability distributions used for the parameters are listed in Table 3. The deterministic values given in Table 1 were taken as the mean value of the normal distribution of a particular parameter. As a result of the analysis, stress-dependent sensitivity indices at one MPa intervals were calculated for each case during loading and unloading.

The propagated uncertainty in the stress-strain curves due to input variability was determined by calculating the strain from the Brinson model with loading the material to a maximum stress value and then loading to the stress-free state of the material.

Table 3 Probability distributions for the model parameters

Parameter	Distribution	Value	Unit
T	Normal	$\mathcal{N}(5, 0.05), \mathcal{N}(12, 0.12),$ $\mathcal{N}(20, 0.20), \mathcal{N}(40, 0.40),$ $\mathcal{N}(60, 0.60),$	°C
θ	Normal	$\mathcal{N}(0.55, 0.0055)$	MPa/°C
D_a	Normal	$\mathcal{N}(67,000, 670)$	MPa
D_m	Normal	$\mathcal{N}(26,300, 263)$	MPa
M_f	Normal	$\mathcal{N}(9.0, 0.09)$	°C
M_s	Normal	$\mathcal{N}(18.4, 0.184)$	°C
A_s	Normal	$\mathcal{N}(34.5, 0.345)$	°C
A_f	Normal	$\mathcal{N}(49.0, 0.49)$	°C
C_M	Normal	$\mathcal{N}(8.0, 0.08)$	MPa/°C
C_A	Normal	$\mathcal{N}(13.8, 0.138)$	MPa/°C
σ_s^{cr}	Normal	$\mathcal{N}(100.0, 1.0)$	MPa
σ_f^{cr}	Normal	$\mathcal{N}(170.0, 1.7)$	MPa
ϵ_L	Normal	$\mathcal{N}(0.067, 0.00067)$	-

Results

Probabilistic analysis demonstrated that small uncertainties introduced to the input parameters with a coefficient of variation of 0.01 resulted in significant variability in the strain values calculated at simulated stress values. The range of the values sampled from the corresponding normal distributions of the input parameters is shown by the parallel coordinate plot in Figure 3. The maximum variability in strain is summarized in Table 4 with consideration given to the operating temperature.
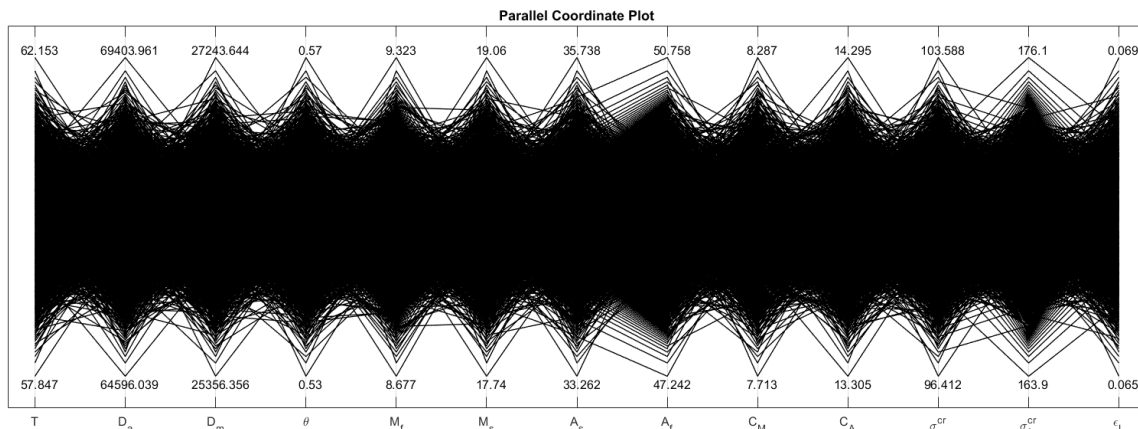

Figure 3 Parallel coordinate plot showing the limits of the parameters tested. (The limits for the temperature is shown for only $T = 60$°C.)

Table 4 Maximum variability in strain over the entire stress-strain curve at an operating temperature

Temperature, T	Max. Variability
$T < M_f$	25-35%
$M_f < T < M_s$	29-42%
$M_s < T < A_s$	66-206%
$A_s < T < A_f$	71-254%
$T > A_f$	75-306%

Uncertainty Analysis

The propagation of uncertainty in the parameters were determined by calculating 5-95% confidence intervals on the obtained stress-strain data (Figure 4). It was observed that the uncertainty in the model showed variation with operating temperature and loading region. When loading and unloading regions were compared, the linear loading regions revealed relatively low variability in strain. At the nonlinear loading regions (detwinning of martensite variants or transformation from austenite to martensite), the variability in strain started to grow at all operating temperatures simulated. The overall observed uncertainty increased with increasing operating temperature and maximum stress.

As mentioned previously, two cases were considered at 60°C. The difference was that in one of the cases, the maximum loading stress was above the critical transition stress for martensite (Figure 4f). As can be seen from the figure, the observed tendency for amplified variability after loading is not present in this case. The variability at the nonlinear loading regions are the same for the same stress values in Figures 4e and 4f, but reaching the critical transition stress during loading decreases the variability band, which remains relatively low until the material returns back to its stress-free state.

Sensitivity Analysis

Sensitivity factors were used to analyse the effect of each parameter on the output of the Brinson model. Figure 5 shows the stress-dependent sensitivity index for each parameter at every stress value simulated with one-MPa increments. In order to observe the overall effect of each parameter, the average sensitivity index for each parameter across all simulated stress values was also calculated (Figure 6). There were no significant interaction effects between the parameters.

It was observed that the sensitivity of the model to its parameters showed variation with changing operating temperature and loading region. The elastic moduli played an important role in determining the behaviour of the model especially in the linear loading region. In that region, depending on the initial martensitic or austenitic phase, the model was sensitive to either D_m or D_a. An exception was for the case when $M_f < T < M_s$; at this temperature the material had a martensite fraction between 0 and 1, which caused the effective modulus to be a combination of 100% austenite and 100% martensite moduli.
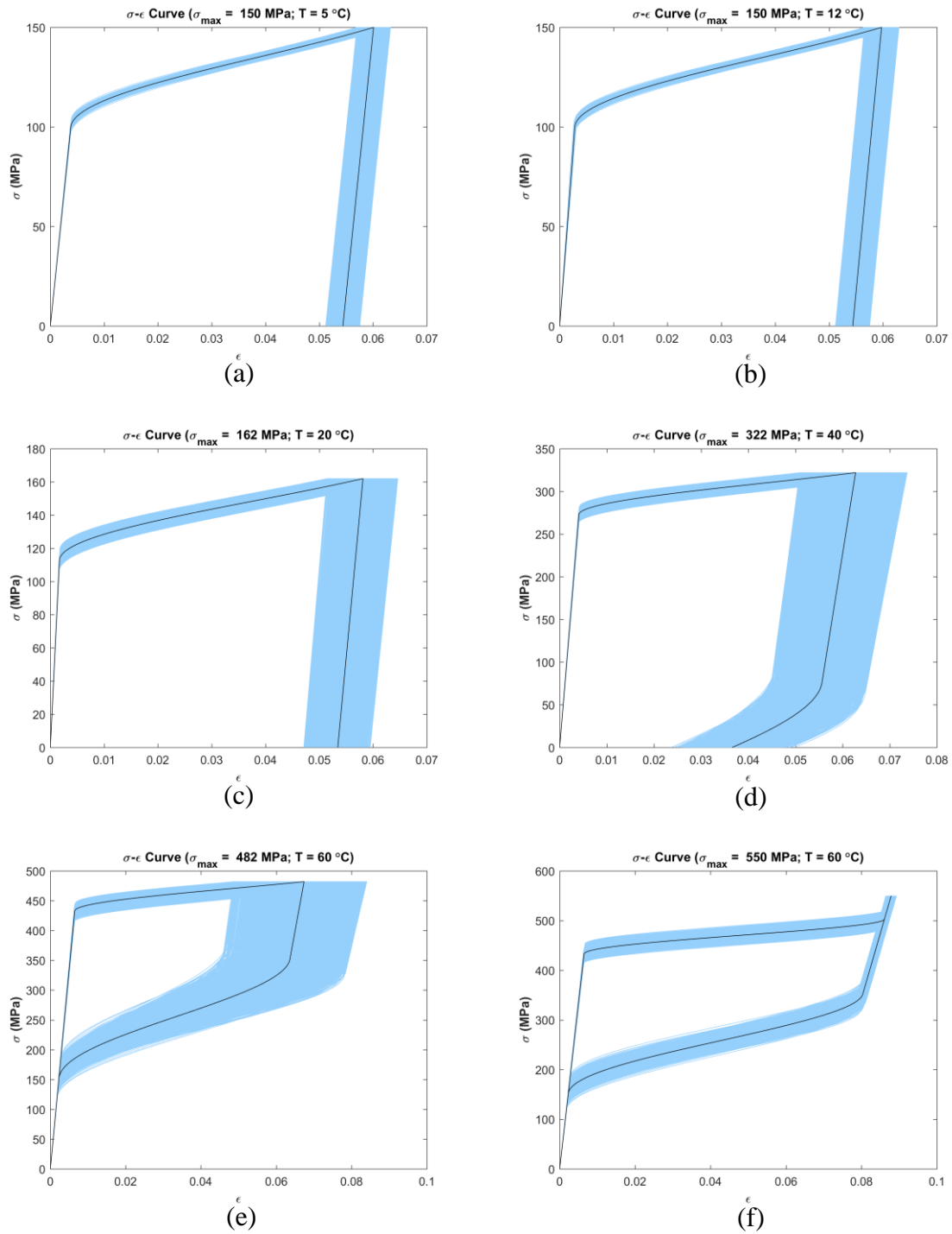
Figure 4 Confidence intervals (5-95 percentile) at simulated temperatures and maximum loading stress (The black line represents the deterministic curve.): (a) $T = 5°C$; $\sigma_{max} = 150$ MPa, (b) $T = 12°C$; $\sigma_{max} = 150$ MPa, (c) $T = 20°C$; $\sigma_{max} = 162$ MPa, (d) $T = 40°C$; $\sigma_{max} = 322$ MPa, (e) $T = 60°C$; $\sigma_{max} = 482$ MPa, and (f) $T = 60°C$; $\sigma_{max} = 550$ MPa$> \sigma_f^{cr} + C_M(T - M_s)$.
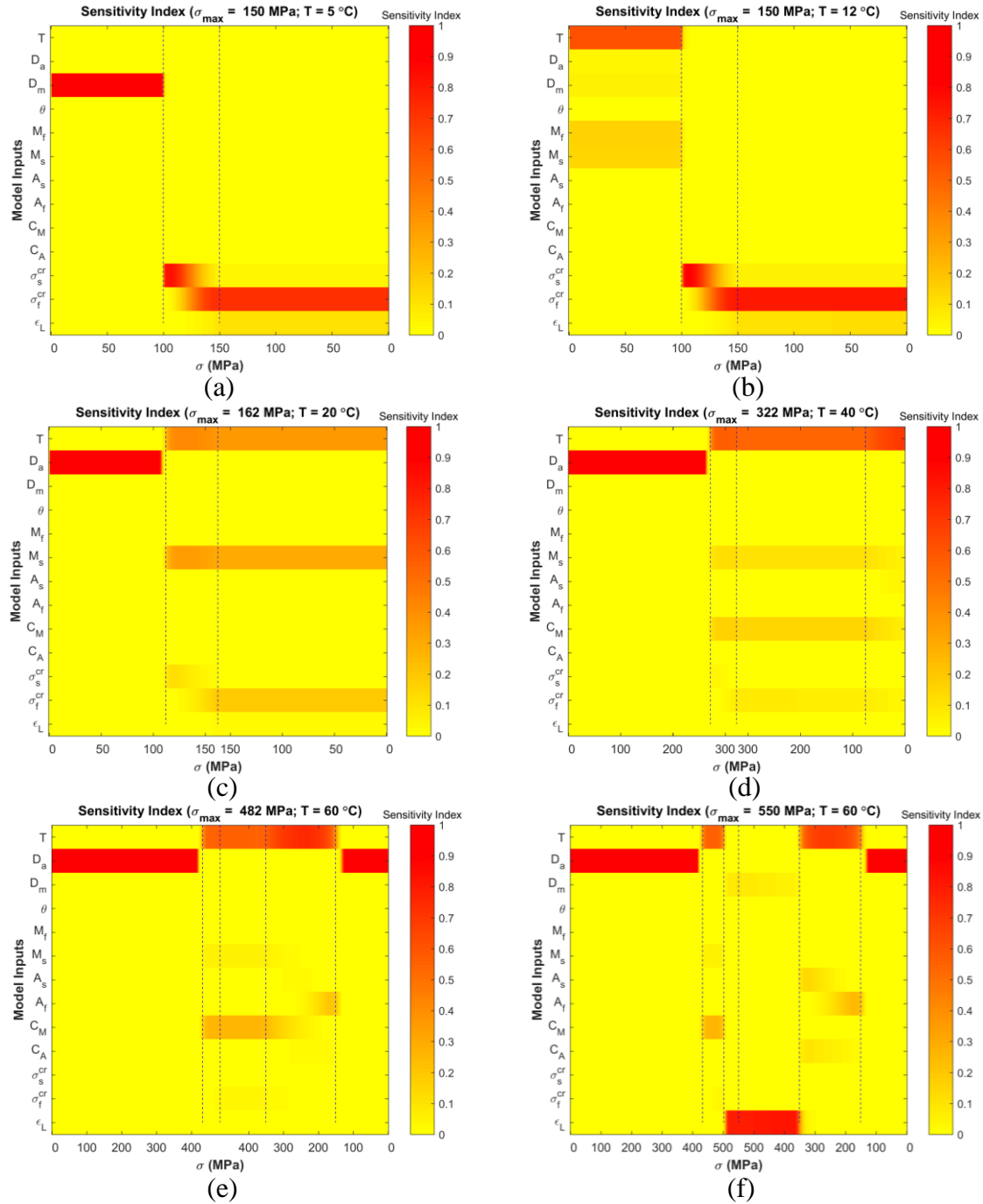
Figure 5 FAST stress-dependent sensitivity index distribution at simulated temperatures. Critical stress values are shown by vertical lines and include the following in the given order (when applicable): $\sigma_s^{cr} + C_M(T - M_s)$ with $C_M = 0$ at $T < M_s$; σ_{max}; $\sigma_f^{cr} + C_M(T - M_s)$; $C_A(T - A_s)$; $C_A(T - A_f)$.
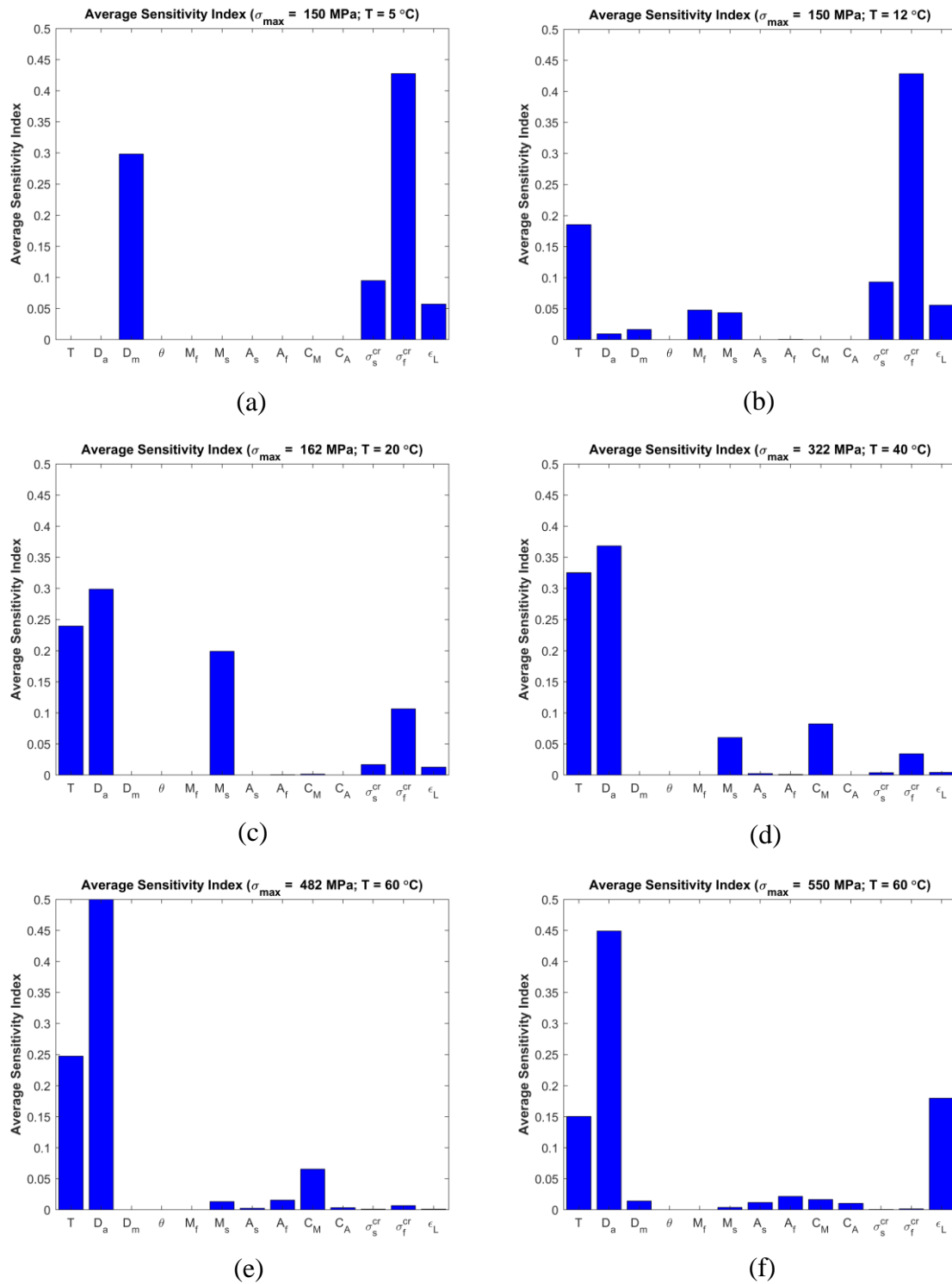
Figure 6 FAST average sensitivity indices at simulated temperatures and maximum loading stress: (a) $T = 5°C$; $\sigma_{max} = 150$ MPa, (b) $T = 12°C$; $\sigma_{max} = 150$ MPa, (c) $T = 20°C$; $\sigma_{max} = 162$ MPa, (d) $T = 40°C$; $\sigma_{max} = 322$ MPa, (e) $T = 60°C$; $\sigma_{max} = 482$ MPa, and (f) $T = 60°C$; $\sigma_{max} = 550$ MPa$> \sigma_f^{cr} + C_M(T - M_s)$.

At the nonlinear loading region (detwinning of martensite variants or transformation from austenite to martensite), the dominant parameter was the temperature at all operating temperatures except when $T < M_s$. For these operating temperatures (5°C and 12°C) , σ_f^{cr} and σ_s^{cr} were important, and that trend continued through unloading. While unloading at the remaining operating temperatures, the model became sensitive to the transition temperatures and C_M. The maximum residual strain (ϵ_L) became a dominant parameter when unloading at 60°C until the critical stress for austenite transition was reached.

The results of the sensitivity analysis were verified by 1) Calculating the sensitivity indices with FAST by removing the uninfluential parameters from the analysis, and 2) Calculating the Sobol's sensitivity indices with all variables presented in Table 3. The results of the FAST analysis were identical to the ones shown in Figure 5, and, therefore, are not repeated here. The Sobol's indices are shown in Figure 7. It is observed that the main effects are in close agreement with the first-order indices obtained from the FAST sensitivity analysis. Additionally, the total effects confirm the observation that the higher-order indices (interactions) do not play a significant role in explaining the variance of the output data.

Discussion

This study demonstrates the use of probabilistic modelling in quantifying the effect of input parameter variabilities on the stress-strain curve as predicted by the one-dimensional Brinson model. This variability in the inputs significantly affects the prediction of the strain during loading and unloading of the material. Therefore, it is crucial to acquire a thorough understanding of which parameters are dominant in the process so that necessary feasible precautions may be taken when determining the model parameters with experimentation. The lack of this knowledge may lead to performance differences between the simulation of a model and its real-life implementation. Simulations using models are cost-effective design tools and expedite a product's development cycle significantly. For instance, when SMAs are used for active control of a structure, simulations can be used to test control strategies and tune the controller gains offline. The reaction of the model to the uncertainties in its inputs, however, can cause misrepresentation of the real-life behaviour of the material, and, therefore, creates less than desired performance outcomes in implementation. This outcome may even be the instability of the overall structure. In the following paragraphs, we discuss the results obtained from the analysis and provide recommendation in order to effectively make use of the Brinson model in applications using SMAs.
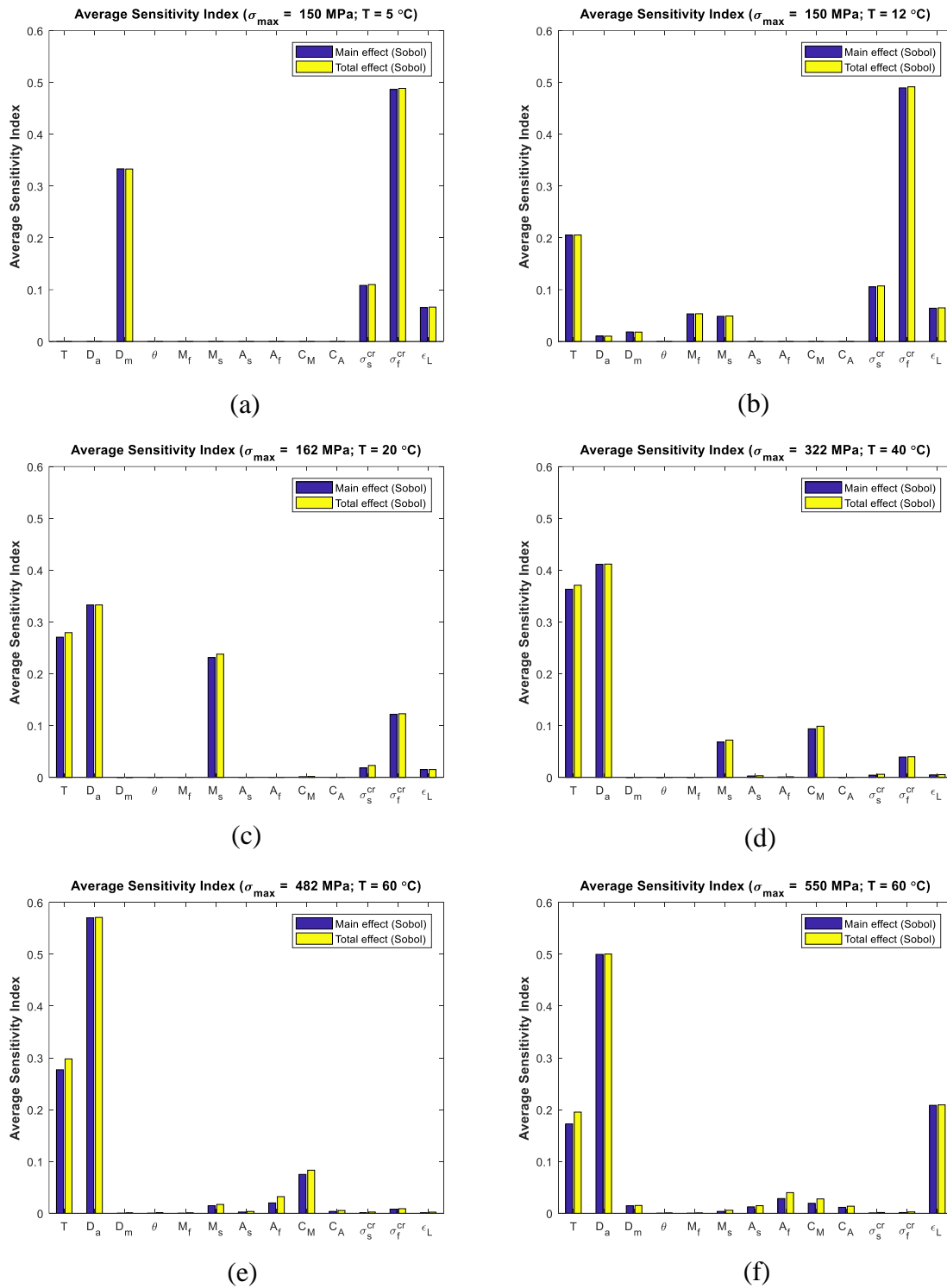
Figure 7 Sobol's average sensitivity indices at simulated temperatures and maximum loading stress: (a) $T = 5°$C; $\sigma_{max} = 150$ MPa, (b) $T = 12°$C; $\sigma_{max} = 150$ MPa, (c) $T = 20°$C; $\sigma_{max} = 162$ MPa, (d) $T = 40°$C; $\sigma_{max} = 322$ MPa, (e) $T = 60°$C; $\sigma_{max} = 482$ MPa, and (f) $T = 60°$C; $\sigma_{max} = 550$ MPa$> \sigma_f^{cr} + C_M(T - M_s)$.

The propagation of uncertainty was observed to change according to the operating temperatures and loading conditions. This is not surprising as the phase transformations in the SMAs are closely related to these variables. Therefore, the portions of the stress-strain curves with an associated phase transformation during loading amplifies the propagated uncertainty. The linear portions of the loading do not amplify the variability as compared to the nonlinear portions. The most variability in strain was observed during unloading after the phase transformation region except for the case when the material was converted to 100% martensite after starting from 100% austenite, which showed somewhat controlled variability. This is probably due to the overall low variability in the linear regions (both loading and unloading). In the linear regions, phase changes do not occur and the model's treatment of these regions relies on less number of parameters as compared to the nonlinear regions when phase transformations occur.

The sensitivity to D_m at temperatures below M_f can be readily explained by the material being in the fully martensitic phase and the slope of the linear loading curve is governed only by D_m. At any temperature above M_f, the material is cooled down from the parent austenitic phase and, therefore, the martensite fraction is less than one. The Brinson model calculates the elastic modulus of the material at any temperature based on Eqn. (3) that includes both the martensitic and austenitic material properties. As a result, D_a gradually becomes an important parameter especially during the loading and unloading as the martensite fraction decreases. Especially, at temperatures $M_s < T$, the model's assumption of no phase transformation between $M_s < T < A_s$ is applicable and D_a is an important parameter as the material is in the austenitic phase. This is observed especially at the linear regions of loading. At temperatures above A_f, exhibiting pseudoelastic behavior, the material starts as austenite and transforms fully back to the same parent phase upon unloading; during the stages at which the material is fully austenite, D_a continues to remain a dominant parameter. Additionally, for temperatures $T < A_s$, σ_f^{cr} and σ_s^{cr} plays an important role as the phase transformations are defined based on these parameters and the calculation of the martensite fraction is highly dependent on their values. For higher temperatures, however, these parameters gradually becomes unimportant as the calculation of martensite fraction is not dependent on the values of the critical stresses. When the material is loaded beyond the critical transformation stress at the finish of martensite variants (σ_f^{cr}) at temperatures above A_f, the parent austenite phase is completely transformed into detwinned martensite, which results in the highest value of the stress-induced martensite fraction at a temperature that had no martensite formation before loading. This causes the transformation tensor to play an important role while calculating stress-strain stress curves and the maximum residual strain ϵ_L becomes dominant as can be observed from Eqn. (4). The model appears to be sensitive the temperature at all simulated cases except for $T < M_f$. The reason is that the calculation of the martensite fraction during phase transformations and in Eqn. (2) does not involve the temperature during isothermal loading and unloading. Finally, M_s is dominant only when the operating temperatures are between $M_s < T < A_s$ as martensite fraction calcualtions in the model include this paremeter as a direct input.

The effect of operating temperature on the variability of outputs was also observed. A general tendency is that the variability in the calculated strain values increases with increasing operating temperature. The reason can be attributed to the temperature range within which phase transformations take place. For instance, when $T < A_s$, the reverse transformation from martensite to austenite does not take place and the resulting variability is less than the operating temperatures that are above austenite start temperature.

The stress-dependent sensitivity indices are especially beneficial when dissecting the dependency of the Brinson model on specific parameters at any stage of the loading and unloading. The initial linear loading stage appears to be most sensitive to the 100% austenite (D_a) and 100% martensite (D_m) moduli of the SMA. When the operating temperature is below martensite finish, the model is most sensitive to D_m as the stress-strain relationship (at isothermal loading) is dominated with this value. When initially fully austenite, however, D_a becomes the dominant parameter as the martensite fraction is zero at this stage. The only case that had the material in a mixed state $(T = 12°C)$, we observed a decrease in the sensitivity of the model to these moduli. Instead, martensite start and finish temperatures along with the operating temperature become important. This can be attributed to the fact that the calculation of the martensite fraction is dependent on these variables, and it is the martensite fraction that defines the contribution of the material moduli to the stress-strain calculation in this linear region. During the phase transformations upon loading critical transition stresses are important at temperatures below austenite finish temperature. Their effect is more prominent for the temperatures below martensite start. Above martensite start temperature, the sensitivity of the model to temperature starts to become noticeable and that effect continues upon unloading.

An interesting finding is the relatively small variability in the case when the material is allowed to convert from 100% austenite to 100% martensite at a temperature above the austenite finish temperature. It is observed that the strain values calculated during the formation of the detwinned martensite for all simulated samples come closer to each other after the stress value exceeds the critical stress for martensite finish (after the effect of the temperature is incorporated). Followed by a non-transition region, the variability remains low as compared to the same region of the curve at the same operating temperature and when the max stress is below $\sigma_f^{cr} + C_M(T - M_s)$. Therefore, the variability in the parameters propagate in a more controlled manner when the material, at temperatures above the austenite finish temperature, is allowed to convert to full martensite before unloading. Although not presented here, the same tendency was observed for all operating temperatures. This can be interpreted as, in the Brinson model, the pseudoelastic behavior of SMAs introduces low output variability when they are loaded above $\sigma_f^{cr} + C_M(T - M_s)$ before unloading. This case was the only one that maximum residual strain became a moderately effective factor in the sensitivity analysis.

Based on the results discussed herein, Table 5 presents the most dominant parameters that affect the variability in the strain values as determined by the Brinson model based on the SMA behaviour (pseudoelastic and shape memory effects) in different temperature

ranges.   Depending on the application, pseudoelastic effect may be utilized to apply constant stress after even large strains. The shape memory effect, on the other hand, is mainly used for actuation by means of recovering the strain due to loading via joule heating or using any other type of heat source. For SMA models that utilize this model, we recommend the resources to be directed towards measuring the material moduli (D_a and D_m), critical transformation stresses (σ_f^{cr} and σ_s^{cr}), martensite start temperature (M_s), operating temperature (T), and maximum residual strain (ϵ_L) with least possible uncertainty as they prescribe the range of variability in the stress-strain curve obtained from the model. The thermal coefficient of expansion for the SMA material (Θ), martensite finish temperature (M_f), austenite start temperature (A_s), austenite finish temperature (A_f), and the slopes of the transition inducing critical stress-temperature curves (C_M, C_A) did not contribute to the variability in the stress-strain curve. These parameters, as described in the manuscript, are: the material moduli (D_a and D_m), critical transformation stresses (σ_f^{cr} and σ_s^{cr}), martensite start temperature (M_s), operating temperature (T), and maximum residual strain (ϵ_L).

It should be noted that parameter correlations were not a limiting factor for the current study. Only potential source of correlation is that the C_M and C_A relate the critical stresses and temperature. However, neither of these parameters are influential parameters at any of the six cases simulated. The temperature and critical stress values were not observed to emerge as influential parameters simultaneously in five out of the six cases simulated. Finally, the lack of experimental data for the determination of these parameters prohibits the establishment of potential correlations.

Table 5 Dominant parameters by operating temperature

Temperature, T	SMA Behavior	Parameter
$T < M_f$		$D_m, \sigma_f^{cr}, \sigma_s^{cr}$
$M_f < T < M_s$	Shape Memory	$\sigma_f^{cr}, \sigma_s^{cr}, T$
$M_s < T < A_s$	Effect	D_a, M_s, T
$A_s < T < A_f$		D_a, T
$T > A_f$ and $\sigma_{max} < \sigma_f^{cr} + C_M(T - M_s)$	Pseudoelastic	D_a, T
$T > A_f$ and $\sigma_{max} > \sigma_f^{cr} + C_M(T - M_s)$	Effect	D_a, T, ϵ_L

Conclusion

This study employed a probabilistic approach for identifying how uncertainties in the input parameters of the Brinson model affect its output. The sensitivity analyses provide a tool to investigate the key input parameters so that resources can be directed towards reducing their variability, and, therefore, increasing the reliability of the model-predicted data. This treatment is important in order to create simulations that accurately represent the real-life behaviour of the material in related applications. As a result of the analysis, as presented by the current study, specific recommendations can be made as to which parameters are dominant in prescribing the variability in the model output. The

systematic approach employed herein can be applied to any model developed for other intelligent materials.

References

Andreasen, G.F. and Hilleman, T.B., 1971. An evaluation of 55 cobalt substituted Nitinol wire for use in orthodontics. *The Journal of the American Dental Association*, *82*(6), pp.1373-1375.

Andreasen, G.F., University of Iowa Research Foundation (UIRF), 1977. *Method and system for orthodontic moving of teeth*. U.S. Patent 4,037,324.

Balta, J.A., Bosia, F., Michaud, V., Dunkel, G., Botsis, J. and Månson, J.A., 2005. Smart composites with embedded shape memory alloy actuators and fibre Bragg grating sensors: activation and control. *Smart materials and structures*, *14*(4), p.457.

Birman, V., 1997. Review of mechanics of shape memory alloy structures. *Applied Mechanics Reviews*, *50*(11), pp.629-645.

Brinson, L.C., 1993. One-dimensional constitutive behavior of shape memory alloys: thermomechanical derivation with non-constant material functions and redefined martensite internal variable. *Journal of intelligent material systems and structures*, *4*(2), pp.229-242.

Brugger, D., Kohl, M., Hollenbach, U., Kapp, A. and Stiller, C., 2006. Ferromagnetic shape memory microscanner system for automotive applications. *International Journal of Applied Electromagnetics and Mechanics*, *23*(1, 2), pp.107-112.

Buehler, W.J. and Wang, F.E., 1968. A summary of recent research on the Nitinol alloys and their potential application in ocean engineering. *Ocean Engineering*, *1*(1), pp.105-120.

Buehler, W.J., Gilfrich, J.V. and Wiley, R.C., 1963. Effect of low-temperature phase changes on the mechanical properties of alloys near composition TiNi. *Journal of applied physics*, *34*(5), pp.1475-1477.

Cho, K.J., Hawkes, E., Quinn, C. and Wood, R.J., 2008, May. Design, fabrication and analysis of a body-caudal fin propulsion system for a microrobotic fish. In *Robotics and Automation, 2008. ICRA 2008. IEEE International Conference on* (pp. 706-711). IEEE.

Cianchetti, M., Licofonte, A., Follador, M., Rogai, F. and Laschi, C., 2014, July. Bioinspired soft actuation system using shape memory alloys. In *Actuators* (Vol. 3, No. 3, pp. 226-244). Multidisciplinary Digital Publishing Institute.

Cukier, R.I., Fortuin, C.M., Shuler, K.E., Petschek, A.G. and Schaibly, J.H., 1973. Study of the sensitivity of coupled reaction systems to uncertainties in rate coefficients. I Theory. *The Journal of chemical physics*, *59*(8), pp.3873-3878.

Cukier, R.I., Levine, HB and Shuler, KE, 1978. Nonlinear sensitivity of multiparameter model systems. *J. Comp. Phys*, *6*, pp.1-42.

Cukier, R.I., Schaibly, J.H. and Shuler, K.E., 1975. Study of the sensitivity of coupled reaction systems to uncertainties in rate coefficients. III. Analysis of the approximations. *The Journal of Chemical Physics*, *63*(3), pp.1140-1149.

Dye, T.E., 1990. *An experimental investigation of the behavior of nitinol* (Doctoral dissertation, Virginia Tech).

Fujita, H., 1989, May. Studies of micro actuators in Japan. In *Robotics and Automation, 1989. Proceedings., 1989 IEEE International Conference on* (pp. 1559-1564). IEEE.

Hartl, D.J. and Lagoudas, D.C., 2007. Aerospace applications of shape memory alloys. *Proceedings of the Institution of Mechanical Engineers, Part G: Journal of Aerospace Engineering*, *221*(4), pp.535-552.

Honma, D. and Miwa, Y., 1985. Iguchi,"Micro Robots and Micro Mechanisms Using Shape Memory Alloy to Robotic Actuators,". *J. of Robotic Systems*, *2*(1), pp.3-25.

Ikuta, K., 1990, May. Micro/miniature shape memory alloy actuator. In *Robotics and Automation, 1990. Proceedings., 1990 IEEE International Conference on* (pp. 2156-2161). IEEE.

Jani, J.M., Leary, M., Subic, A. and Gibson, M.A., 2014. A review of shape memory alloy research, applications and opportunities. *Materials & Design (1980-2015)*, *56*, pp.1078-1113.

Kaufman, J.A., Geller, S.C., Brewster, D.C., Fan, C.M., Cambria, R.P., LaMuraglia, G.M., Gertler, J.P., Abbott, W.M. and Waltman, A.C., 2000. Endovascular repair of abdominal aortic aneurysms: current status and future directions. *American Journal of Roentgenology*, *175*(2), pp.289-302.

Khouri, R.K., Brava LLC, 2002. *Method and apparatus for expanding soft tissue with shape memory alloys*. U.S. Patent 6,478,656.

Konh, B., Datla, N.V. and Hutapea, P., 2015. Feasibility of shape memory alloy wire actuation for an active steerable cannula. *Journal of Medical Devices*, *9*(2), p.021002.

Kujala, S., Ryhänen, J., Jämsä, T., Danilov, A., Saaranen, J., Pramila, A. and Tuukkanen, J., 2002. Bone modeling controlled by a nickel–titanium shape memory alloy intramedullary nail. *Biomaterials*, *23*(12), pp.2535-2543.

Kuribayashi, Katsutoshi. "Millimeter size joint actuator using shape memory alloy." In *Micro Electro Mechanical Systems, 1989, Proceedings, An Investigation of Micro Structures, Sensors, Actuators, Machines and Robots. IEEE*, pp. 139-144. IEEE, 1989.

Leary, M., Huang, S., Ataalla, T., Baxter, A. and Subic, A., 2013. Design of shape memory alloy actuators for direct power by an automotive battery. *Materials & Design*, *43*, pp.460-466.

Liang, C., 1990. *The constitutive modeling of shape memory alloys* (Doctoral dissertation, Virginia Tech).

Lin, H.T., Leisk, G.G. and Trimmer, B., 2011. GoQBot: a caterpillar-inspired soft-bodied rolling robot. *Bioinspiration & biomimetics*, *6*(2), p.026007.

Machado, L.G. and Savi, M.A., 2003. Medical applications of shape memory alloys. *Brazilian journal of medical and biological research*, *36*(6), pp.683-691.

Mantovani, D., 2000. Shape memory alloys: Properties and biomedical applications. *Jom*, *52*(10), pp.36-44.

Morgan, N.B., 2004. Medical shape memory alloy applications—the market and its products. *Materials Science and Engineering: A*, *378*(1-2), pp.16-23.

Morgansen, K.A., Duidam, V., Mason, R.J., Burdick, J.W. and Murray, R.M., 2001. Nonlinear control methods for planar carangiform robot fish locomotion. In *Robotics and Automation, 2001. Proceedings 2001 ICRA. IEEE International Conference on* (Vol. 1, pp. 427-434). IEEE.

Musialek, J., Filip, P. and Nieslaník, J., 1998. Titanium-nickel shape memory clamps in small bone surgery. *Archives of orthopaedic and trauma surgery*, *117*(6-7), pp.341-344.

Peng, F., Jiang, X.X., Hu, Y.R. and Ng, A., 2005, March. Application of shape memory alloy actuators in active shape control of inflatable space structures. In *Aerospace Conference, 2005 IEEE* (pp. 1-10). IEEE.

Perkins, J., Edwards, G.R., Such, C.R., Johnson, J.M. and Allen, R.R., 1975. Thermomechanical characteristics of alloys exhibiting martensitic thermoelasticity. In *Shape memory effects in alloys* (pp. 273-303). Springer, Boston, MA.

Pianosi, F., Sarrazin, F. and Wagener, T., 2015. A Matlab toolbox for global sensitivity analysis. *Environmental Modelling & Software*, *70*, pp.80-85.

Prahlad, H. and Chopra, I., 2001, August. Design of a variable twist tilt-rotor blade using shape memory alloy (SMA) actuators. In *Smart Structures and Materials 2001: Smart Structures and Integrated Systems* (Vol. 4327, pp. 46-60). International Society for Optics and Photonics.

Roh, J.H., Han, J.H. and Lee, I., 2005, May. Finite element analysis of adaptive inflatable structures with SMA strip actuator. In *Smart Structures and Materials 2005: Smart Structures and Integrated Systems* (Vol. 5764, pp. 460-472). International Society for Optics and Photonics.

Ryhänen, J., Kallioinen, M., Tuukkanen, J., Junila, J., Niemelä, E., Sandvik, P. and Serlo, W., 1998. In vivo biocompatibility evaluation of nickel-titanium shape memory metal alloy: Muscle and perineural tissue responses and encapsule membrane thickness. *Journal of Biomedical Materials Research: An Official Journal of The Society for Biomaterials, The Japanese Society for Biomaterials, and the Australian Society for Biomaterials*, *41*(3), pp.481-488.

Sanders, A.E., Sanders, J.O. and More, R.B., Sanders Albert E, Sanders James O and More Robert B, 1994. *Nitinol spinal instrumentation and method for surgically treating scoliosis*. U.S. Patent 5,290,289.

Sanders, J.O., Sanders, A.E., More, R. and Ashman, R.B., 1993. A preliminary investigation of shape memory alloys in the surgical correction of scoliosis. *Spine*, *18*(12), pp.1640-1646.

Schmerling, M.A., Wilkov, M.A., Sanders, A.E. and Woosley, J.E., 1976. Using the shape recovery of nitinol in the Harrington rod treatment of scoliosis. *Journal of biomedical materials research*, *10*(6), pp.879-892.

Seok, S., Onal, C.D., Cho, K.J., Wood, R.J., Rus, D. and Kim, S., 2013. Meshworm: a peristaltic soft robot with antagonistic nickel titanium coil actuators. *IEEE/ASME Transactions on mechatronics*, *18*(5), pp.1485-1497.

Simone, F., York, A. and Seelecke, S., 2015, March. Design and fabrication of a three-finger prosthetic hand using SMA muscle wires. In *Bioinspiration, Biomimetics, and Bioreplication 2015* (Vol. 9429, p. 94290T). International Society for Optics and Photonics.

Song, G., Chaudhry, V. and Batur, C., 2003. Precision tracking control of shape memory alloy actuators using neural networks and a sliding-mode based robust controller. *Smart materials and structures*, *12*(2), p.223.

Suzuki, M., Tokai Rika Co Ltd, 1986. *Rotatable door mirror for a motor vehicle*. U.S. Patent 4,626,085.

Tanaka, K., 1986. A thermomechanical sketch of shape memory effect: one-dimensional tensile behavior. *Res. Mechanica*, *18*, pp.251-263.

Tanaka, M., Hirano, K., Goto, H., Namima, T., Uchi, K., Jiang, Z.W., Matsuki, H., Tanahashi, Y., Orikasa, S. and Chonan, S., 1999. Artificial SMA valve for treatment of urinary incontinence: upgrading of valve and introduction of transcutaneous transformer. *Bio-medical materials and engineering*, *9*(2), pp.97-112.

Triantafyllou, M.S. and Triantafyllou, G.S., 1995. An efficient swimming machine. *Scientific american*, *272*(3), pp.64-70.

Uflacker, R. and Robison, J., 2001. Endovascular treatment of abdominal aortic aneurysms: a review. *European radiology*, *11*(5), pp.739-753.

Vena, P., Franzoso, G., Gastaldi §, D., Contro, R. and Dallolio, V., 2005. A finite element model of the L4–L5 spinal motion segment: biomechanical compatibility of an interspinous device. *Computer methods in biomechanics and biomedical engineering*, *8*(1), pp.7-16.

Wei, Z.G., Sandstroröm, R. and Miyazaki, S., 1998. Shape-memory materials and hybrid composites for smart systems: Part I Shape-memory materials. *Journal of Materials Science*, *33*(15), pp.3743-3762.

Wever, D., Elstrodt, J., Veldhuizen, A. and v Horn, J., 2002. Scoliosis correction with shape-memory metal: results of an experimental study. *European Spine Journal*, *11*(2), pp.100-106.

Williams, E.A., Shaw, G. and Elahinia, M., 2010. Control of an automotive shape memory alloy mirror actuator. *Mechatronics*, *20*(5), pp.527-534.

Willy, A. and Low, K.H., 2005, June. Development and initial experiment of modular undulating fin for untethered biorobotic AUVs. In *Robotics and Biomimetics (ROBIO). 2005 IEEE International Conference on* (pp. 45-50). IEEE.

Zychowicz, R., Britax Geco SA, 1992. *Exterior view mirror for a motor vehicle*. U.S. Patent 5,166,832.